Oncology Research

Tech Science Press

http://doi.org/10.32604/or.2026.083630

ARTICLE

Altered Expression of UFMylation Pathway Proteins Is Linked with Cancer Stem Cell Features and Aggressive Clinical Phenotype of Head and Neck Cancer

Kristina Vukovic Derfi[1], Marko Tarle[2,3], Koraljka Hat[2,3], Tea Vasiljevic[1], Danko Müller[4,5], Ivica Luksic[2,5] and Tanja Matijevic Glavan[1,*]

[1]Division of Molecular Medicine, Rudjer Boskovic Institute, Zagreb, Croatia
[2]Department of Maxillofacial Surgery, Dubrava University Hospital, Zagreb, Croatia
[3]School of Dental Medicine, University of Zagreb, Zagreb, Croatia
[4]Department of Pathology and Cytology, Dubrava University Hospital, Zagreb, Croatia
[5]School of Medicine, University of Zagreb, Zagreb, Croatia
*Corresponding Author: Tanja Matijevic Glavan. Email: tmatijev@irb.hr

Received: 07 April 2026; Accepted: 18 August 2026; Online first: 25 August 2026

ABSTRACT: Objectives: Head and neck squamous cell carcinoma (HNSCC), with oral squamous cell carcinoma (OSCC) comprising approximately 90% of cases, is a highly aggressive cancer characterized by frequent recurrence, therapy resistance, and poor prognosis, all largely attributed to the presence of cancer stem cells (CSCs). The UFMylation pathway, a recently described post-translational modification, has been implicated in the regulation of cancer cell survival, proliferation, and stemness; however, its clinical significance in HNSCC remains poorly understood. In the present study, we aimed to examine the correlation between dysregulated UFMylation components and both the clinical presentation and CSC-related phenotypes in HNSCC. **Methods:** The expression of UFM1-specific peptidase 2 (UFSP2) protein was evaluated in tumor and normal tissues from 54 oral squamous cell carcinoma (OSCC) patients and correlated with clinicopathological features. The expression of stemness markers, UFMylation-related genes/proteins and UFMylation substrates was also assessed. Functional effects of Ubiquitin-Like Modifier Activating Enzyme 5 (UBA5) inhibition were examined in tumor spheres, including survival, apoptosis, autophagy, and ferroptosis-related markers. Bioinformatic analyses were performed to explore associations between UFMylation proteins, stemness/epithelial–mesenchymal transition (EMT) markers, iron metabolism-related markers, and pathological stage. **Results:** UFSP2 expression levels varied considerably among tumors, with both overexpression and downregulation consistently associated with advanced OSCC clinical severity. UFSP2-overexpressing cohort exhibited broad up-regulation of stemness markers cluster of differentiation 133 (CD133) and octamer-binding transcription factor 4 (OCT4), whilst UFSP2-downregulated tumors consistently displayed at least one upregulated stemness marker. The most advanced cases demonstrated elevated UFM1-conjugating enzyme 1 (UFC1) and UBA5 levels, typically alongside increased DDRGK domain-containing protein 1 (DDRGK1) and UFMylation substrate expression. UBA5 inhibition demonstrated a distinct, dose-dependent impact on tumor spheres: whereas low concentrations promoted tumor sphere survival, induced autophagy, and upregulated stemness markers, high concentrations significantly impaired sphere viability, triggered ferroptosis, and resulted in total sphere elimination. Bioinformatic analyses further demonstrated tumor-specific correlations between UBA5 and stemness markers, as well as a significant association between the ferroptosis-related gene transferrin receptor 1 (TfR1) and pathological stage in HNSCC. **Conclusion:** Our findings link a dysregulated UFMylation system to increased stemness, iron metabolic shifts, and aggressive clinical phenotype of HNSCC, highlighting a functional role for UFMylation and ferroptosis-related pathways in HNSCC biology. These results underscore the importance of considering the dose-dependent effects of UBA5 modulation when investigating the consequences of perturbing this pathway.

Copyright © 2026 The Authors. Published by Tech Science Press. This work is licensed under a Creative Commons Attribution 4.0 International License, which permits unrestricted use, distribution, and reproduction in any medium, provided the original work is properly cited.

KEYWORDS: Autophagy; cancer stem cells; cancer therapy; ferroptosis; head and neck squamous cell carcinoma; UFMylation

1 Introduction

Cancer stem cells (CSCs) are a subpopulation of cells within tumors that drive tumor initiation, growth, and treatment resistance. Similar to normal stem cells, CSCs possess the ability to self-renew and differentiate into different cell types, enabling them to either generate more CSCs or differentiate into other types of cancer cells that form the tumor bulk. CSCs are also implicated in tumor recurrence due to their resistance to many conventional cancer treatments, such as chemotherapy and radiation therapy. Therefore, they may persist even after the treatment and cause cancer relapse. Additionally, CSCs can induce and support metastasis. It has been demonstrated that they play a role in the tumor microenvironment to coordinate the metastasis cascade through interactions with tumor microenvironment cellular components. They can either aid in creating new metastatic sites, known as a pre-metastatic niche, or promote dissemination of malignant cells by generating a growth-supportive niche, as well as promote angiogenesis to sustain the growth of the secondary tumor [1].

UFMylation system, also known as the ubiquitin-fold modifier 1 (UFM1) conjugation system, is a recently discovered cellular process similar to ubiquitination. It is a type of post-translational modification essential for maintaining cell homeostasis under various cellular stress conditions. UFM1 is post-translationally attached to lysine residues on substrates through a system of enzymes conserved in most eukaryotes: Ubiquitin-Like Modifier Activating Enzyme 5 (UBA5), Ubiquitin-Fold Modifier Conjugating Enzyme 1 (UFC1), and UFM1 Specific Ligase 1 (UFL1), identified as the E1, E2, and E3 enzymes, respectively. UFM1 Specific Peptidase 1 (UFSP1) and UFM1 Specific Peptidase 2 (UFSP2) are the UFM1-specific proteases, and their function is the activation of UFM1, but also the cleavage of UFM1 from the target protein, which enables the recycling of both UFM1 and its substrate [2]. In cancer, its role is still unknown: UFMylation can have both tumor-promoting and tumor-suppressive effects. In breast and pancreatic cancer, UFMylation induces survival and progression; however, in gastric cancer, UFBP1 increases the sensitivity of cancer cells to cisplatin [3]. Due to these contradictory results and possible tissue-specific functions, more research is needed to understand the full role of UFMylation in cancer development and progression.

Head and neck squamous cell carcinoma (HNSCC) is the 6th most common cancer in the world, which arises from the mucosal epithelium of the oral cavity, pharynx, and larynx. Oral squamous cell carcinoma (OSCC) is considered the most common subtype of HNSCC, accounting for ap-proximately 90% of all cases. Oral cavity and laryngeal cancers are most commonly associated with tobacco consumption, alcohol abuse, or both, whereas pharyngeal cancers are attributed to infection with human papillomavirus (HPV). Management of this cancer generally involves surgery, radiotherapy, and chemotherapy, as well as targeted treatments (cetuximab) and recent advancements in immunotherapy (pembrolizumab and nivolumab) [4]. Head and neck cancer treatment is unsuccessful in 50% of cases despite treatment advances. The clinical challenges of HNSCC—namely metastasis and relapse—are largely attributed to the presence of CSCs [5]. Given their role in therapy resistance, uncovering specific molecular markers is vital. Having previously identified the UFMylation pathway as a key regulator of HNSCC CSCs through Sp1-mediated expression [6], our aim in this study was to explore how UFMylation genes and proteins contribute to the CSC phenotype.

2 Materials and Methods

2.1 Patients Samples

Tumor and matched adjacent histologically normal tissue samples were collected from 54 patients with primary oral cavity squamous cell carcinoma (OCSCC) admitted to the Department of Maxillofacial Surgery, Clinical Hospital Dubrava, Zagreb, Croatia. The tissue has been stored in liquid nitrogen immediately after surgery, and afterwards moved to -80°C freezer where it remained until the protein/RNA isolation. The study was conducted in accordance with the Declaration of Helsinki and approved by the Ethics Committee of Clinical Hospital Dubrava, Zagreb, Croatia (No. 2020/2602-02, date: 26.02.2020). Informed patient consent was obtained prior to surgery. All patients underwent the same primary therapeutic approach, surgical resection of the primary tumor with simultaneous neck dissection, to minimize treatment-related heterogeneity. None of the patients had received any previous oncological treatment, ensuring a treatment-naïve cohort and excluding therapy-related effects on tumor biology as a confounding factor. To address HPV-related confounding, HPV status was determined for every tumor by p16 immunohistochemistry on formalin-fixed paraffin-embedded tumor sections, in accordance with current clinical practice for HNSCC. Inclusion criteria were: (a) adults aged $\geq$ 18 years; (b) histopathologically confirmed primary squamous cell carcinoma of the oral cavity; (c) primary surgical treatment consisting of resection of the primary tumor together with neck dissection, the type and extent of which (selective, modified radical, or radical) was determined according to clinical nodal status and characteristics of the primary tumor; (d) availability of fresh-frozen tumor tissue and matched adjacent normal tissue of sufficient quantity and quality for molecular analyses; (e) complete clinical, radiological and pathological documentation, including TNM stage, tumor size, perineural and lymphovascular invasion, bone infiltration, lymph node status with extranodal extension, surgical margins, and risk factor exposure (smoking and alcohol consumption) and (f) signed written informed consent obtained prior to surgery. Exclusion criteria were: (a) any prior radiotherapy of the head and neck region; (b) any previous or synchronous malignancy of the head and neck; (c) any previous treatment for head and neck cancer, including neoadjuvant chemotherapy, radiotherapy, immunotherapy or targeted therapy (i.e., only treatment-naïve patients were included); (d) recurrent disease at the time of surgery; (e) distant metastases at presentation; and (f) incomplete medical documentation or insufficient tissue for downstream analyses.

2.2 Protein and RNA Isolation

RNA and proteins were isolated after mincing the tissue in liquid nitrogen by NucleoSpin RNA/Protein (Mini kit for RNA and protein purification, Macherey-Nagel, Dueren, Germany) according to the manufacturer's instructions. Briefly, after the homogenization of the samples, cells were lysed, filtered by centrifugation, and centrifuged again after the addition of ethanol. Then, for RNA isolation, RNA was bound to the column, followed by on-column DNase digestion, washing, and RNA elution. For protein isolation, the flow-through was precipitated, washed, and the protein pellet was dried. Protein concentration was determined by Bradford assay (Bradford Protein Assay, Bio-Rad, Hercules, CA, USA).

2.3 Western Blot

Proteins were transferred onto a 0.2 μm nitrocellulose membrane as described previously [7]. The membranes were blocked with 2% nonfat dry milk/2% BSA combination and stained with primary antibodies: anti-UFSP2 (1:1000; sc-376084, Santa Cruz Biotechnology, Inc., Dallas, TX, USA), DDRGK1 (1:3000; 21445-1-AP, Proteintech, Manchester, UK), and GAPDH (1:1000; #5174, Cell Signaling Technology, Danvers, MA,

USA). Membranes were also stained with Amido black as a loading control. Afterwards, the membranes were stained with an appropriate peroxidase-conjugated secondary antibody, anti-rabbit IgG (1:5000; #7074, Cell Signaling Technology, Danvers, MA, USA) and anti-mouse IgG (1:3000; NA931V, Amersham, Cytiva, Marlborough, MA, USA), and visualized with the chemiluminescent system Western Lightning® Plus ECL (Perkin Elmer, Waltham, MA, USA). Images were obtained by using Alliance Q9 mini (UVitec, Cambridge, UK).

2.4 qPCR

1 μg of RNA was used as a template for cDNA synthesis reaction by TaqMan® Reverse Transcription Reagents Kit (Applied Biosystems, Branchburg, NJ, USA) and diluted 10 times in qH_2O. The PCR reactions were performed with Sybr® Green PCR Master Mix (SsoAdvanced Universal SYBR Green Supermix, Bio-Rad, Hercules, CA, USA) on a QuantStudio 3 PCR Detection System (Applied Biosystems, Waltham, MA, USA) as described previously [7]. The following amplification program was used: 95°C for 30 s (initial denaturation), 95°C for 30 s (denaturation), 62°C for 30 s and 60°C for 30 s (annealing and elongation).

Primer sequences are: OCT4-F: 5′-GTGGAGGAAGCTGACAACAA-3′, OCT4-R: 5′-ATTCTCCAGGTTG CCTCTCA-3′; ABCG2-F: 5′-TACCTGTATAGTGTACTTCAT-3′, ABCG2-R: 5′-GGTCATGAGAAGTGTTGC TA-3′; CD133-F: 5′-CAGAGTACAACGCCAAACCA-3′, CD133-R: 5′-AAATCACGATGAGGGTCAGC-3′; UFM1-F: 5′-GGCTGCCGTACAAAGTACTCA-3′, UFM1-R: 5′-TTCCATCATTGGTAATAATTGCAC-3′; UFC1-F: 5′-TTTGGACTAGCTCATCTCATGG-3′, UFC1-R: 5′-GAATCAGATCAGGGATTTCCAC-3′; UBA5-F: 5′-CAGCACTGCCTAAACAAGAGG-3′, UBA5-R: 5′-TGAAACCTCAGATACCAGCTCA-3′; 28S-F: 5′-TTGAAA ATCCGGGGGAGAG-3′, 28S-R: 5′-ACATTGTTCCAACATGCCAG-3′; SLC7A11-F:5′-TCTCCAAAGGAGGT TACCTGC-3′, SLC7A11-R: 5′-AGACTCCCCTCAGTAAAGTGAC-3′; TFRC-F: 5′-ACCATTGTCATATACCC GGTTCA-3′, TFRC-R: 5′-CAATAGCCCAAGTAGCCAATCAT-3′; GPX4-F: 5′-GAGGCAAGACCGAAGTAA ACTAC-3′, GPX4-R: 5′-CCGAACTGGTTACACGGGAA-3′; ACSL4-F: 5′-GCTATCTCCTCAGACACACCGA-3′, ACSL4-R: 5′-AGGTGCTCCAACTCTGCCAGTA-3′.

2.5 Cells and Reagents

The human HNSCC-derived cell line Detroit 562 (batch No. 70004014, 2018, ATCC, Manassas, VA, USA) was routinely tested for mycoplasma, and low-passage-number cells were used to form tumor spheres, which were maintained as previously described [6]. UBA5 inhibitor DKM 2-93 (cat. No. S5841) was obtained from Selleckchem (Houston, TX, USA).

2.6 Cytotoxicity Assay

Proliferation of tumor spheres was measured by ViaLight™ Plus Cell Proliferation and Cytotoxicity BioAssay Kit (Lonza, Basel, Switzerland) according to the manufacturer's instructions, as described previously [6]. The luminescence was measured by Tecan Spark microplate reader (Tecan, Männedorf, Switzerland).

2.7 Malondialdehyde (MDA) Determination

For positive control, Detroit 562 cells were treated with 500 μM $CuSO_4$ to induce lipid peroxidation. MDA was determined in supernatants and in cells. The cells were sonicated to release MDA and centrifuged for 10 min at 12,100× *g*. 90 μL of supernatant/cell sample/standard was mixed with 25 μL of qH_2O, 25 μL of thiobarbituric acid (TBA) and 75 μL of 1% H_3PO_4. After 30 min at 90°C, the samples were cooled on ice and transferred to a black 96-well plate. The fluorescence was measured at Ex 515 nm and Em 556 nm on Tecan

Spark microplate reader (Tecan, Männedorf, Switzerland). All values were normalized to protein levels, which were determined by Bradford assay (Bradford Protein Assay, Bio-Rad, Hercules, CA, USA).

2.8 Bioinformatic Analysis

For correlation studies, we have used GEPIA, accessed in July 2025, a web server that extracts data from the Cancer Genome Atlas (TCGA) data portal and the GTEx database of normal tissues (http://gepia.cancer-pku.cn). We have used standard parameters (Pearson coefficient) and analyzed the correlation of the UBA5 with stemness markers ALDH1A1, SOX2, Nanog, ZEB1, KLF4, and OCT4, as well as all proteins from the UFMylation system and transferrin receptors (TfR1 and TfR2).

2.9 Statistics

All cell culture experiments have been performed in at least three biological triplicates. Associations between categorical variables were assessed using Fisher's exact test. Odds ratio (OR) with 95% confidence interval (CI) was calculated to estimate the strength of association. Continuous variables were compared between groups using a two-tailed Student's t-test or Welch's t-test, as appropriate, and the results are given as the mean ± SD. p-values < 0.05 were considered statistically significant. Associations between UFSP2 expression and binary clinicopathological features were further evaluated by logistic regression. Owing to the small sample size and rare-event/quasi-separation conditions, Firth's penalized-likelihood logistic regression was used, with profile-likelihood 95% confidence intervals. The pre-specified primary exposure was reduced UFSP2 (fold-change ≤ 0.5) versus not reduced, with the three features identified in Fig. 1D (tumor size > 4 cm, extranodal extension, depth of invasion > 1 cm) as primary outcomes; multivariable models adjusted for established risk-factor exposure (smoking and/or alcohol use vs. neither). A Bonferroni-corrected threshold of $p < 0.0167$ was applied for the three primary outcomes. The statistical analysis was performed in MS Excel, and Past 4.03.

3 Results

3.1 UFSP2 and DDRGK1 Have Altered Expression in the Tissue of Patients with Severe Clinical Presentation of HNSCC

We have explored the expression of UFSP2 in 54 HNSCC patients' tissues (Supplementary Fig. S1). Clinicopathological characteristics of the patients are shown in Supplementary Table S1. We have determined that UFSP2 was overexpressed in tumor tissue from eight patients compared with control normal tissue (normalized expression to GAPDH was over 2.0) (Supplementary Table S2).

Many of the cases had extremely high overexpression of UFSP2, reaching 68-fold relative expression. Interestingly, these eight cases all had severe clinical presentations, most being T4 stage with features such as perineural invasions, bone infiltrations, metastasis, and in one case, even two primary tumors in the oral cavity. Overall, 63% (5/8) of them classified as T3 or T4 stage with tumors larger than 3 cm in 50% of the cases (4/8), and perineural invasion (PI) was present in 75% (6/8) of the cases (Table 1). We further explored the UFMylation system protein DDRGK1 in these cases and determined that DDRGK1 expression was changed in 6/8 (75%) of them (Fig. 1A).

Table 1: Clinical features of the patients.

Patient No.	pN Status	No. of Metastases	ENE	PVI	LVI	PNI	Bone Invasion	mOSCC	TNM	HPV	Alcohol	Tobacco	Recurrence	Survival Status
3001	pN+	2	No	No	No	Yes	Yes	No	T4aN2bM0	Negative	Yes	Yes	Yes	Dead
3005	pN+	1	Yes	Yes	Yes	No	No	No	pT3N2aM0	Negative	Yes	Yes	Yes	Dead
3010	pN+	8	Yes	Yes	Yes	Yes	No	No	pT2N3bM0	Negative	No	No	Yes	Alive
3015	pN0	0	No	No	No	Yes	Yes	No	T4aN0M0	Negative	Yes	Yes	No	Alive
3021	pN0	0	No	No	No	No	Yes	Yes	T4aN0M0	Negative	No	No	No	Alive
3022	pN0	0	No	No	No	Yes	No	No	T2N0M0	Negative	No	Yes	No	Alive
3028	pN0	0	No	No	No	No	No	No	T2N0M0	Positive	Yes	Yes	No	Alive
3052	pN+	3	Yes	Yes	Yes	Yes	No	No	T4aN3bM0	Negative	Yes	Yes	Yes	Dead
3053	pN+	6	Yes	Yes	Yes	Yes	Yes	No	T4aN3bM0	Negative	No	No	Yes	Dead

Note: OSCC—Oral Squamous Cell Carcinoma, pN0—No regional lymph node metastases. pN+—Presence of regional lymph node metastases. ENE (Extranodal Extension)—Extranodal tumor spread beyond the lymph node capsule. PVI (Perivascular Invasion)—Tumor invasion into tissues surrounding blood vessels. LVI (Lymphovascular Invasion)—Presence of tumor cells within lymphatic or blood vessels. PNI (Perineural Invasion)—Tumor invasion along or within nerves. mOSCC—multifocal oral SCC.

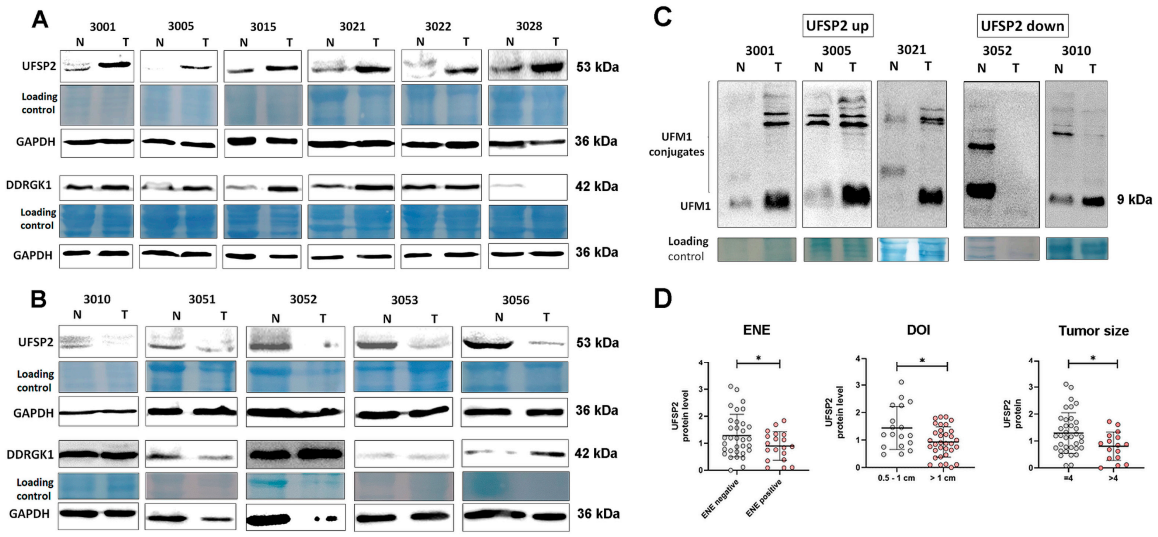

Figure 1: The expression of UFSP2 and DDRGK1 proteins in head and neck squamous cell carcinoma (HNSCC). (**A**,**B**) Representative Western blots show differential expression of UFSP2 and DDRGK1 proteins between paired tumor (T) and adjacent normal (N) tissue samples from patients with clinically aggressive HNSCC. Expression of DDRGK1 in paired normal (N) and tumor (T) tissues from HNSCC patients with (**A**) high overexpression and (**B**) significant downregulation of UFSP2. Amido black staining and GAPDH protein expression were used as a loading control; n = 3 independent experiments. (**C**) UFMylation status of tissues with UFSP2-upregulation (UFSP2 up) and UFSP-downregulation (UFSP2 down). Amido black staining was used as a loading control. (**D**) Association between UFSP2 protein expression and clinicopathological characteristics in 54 head and neck squamous cell carcinoma (HNSCC) patients. Dot plots show the analysis of normalized UFSP2 protein expression in HNSCC patient samples stratified by ENE (extranodal extension) status, DOI (depth of invasion) status, and tumor size. UFSP2 protein levels were quantified relative to GAPDH expression and plotted as individual patient values. Data were represented as dot plots and analyzed by Welch's *t*-test (*$p < 0.05$). ENE—extranodal extension, DOI—depth of invasion.

Eight patients exhibited significantly diminished UFSP2 levels, which also correlated with an aggravated clinical phenotype. A patient with extremely reduced UFSP2 expression (10 times) had exceptionally severe clinical manifestation of the disease with perineural invasion, a conglomerate of positive lymph nodes, three nodes with extranodal extension (ENE), and the patient soon developed a relapse (Patient 3010). We have divided the patients into two groups: the first group exhibited UFSP2 overexpression (Fig. 1A), whereas the second group showed downregulation (Fig. 1B). DDRGK1 was also evaluated in all tested patients, and its expression was found to be deregulated (either higher than 1.5 or lower than 0.5 compared to the normal tissue) in 52% of the samples (Supplementary Fig. S2). Statistical significance was assessed in Western blot results for UFSP2 and DDRGK1 expression (Supplementary Figs. S3 and S4).

UFMylation status was significantly changed in the tissue of the patients with altered UFSP2 expression (either upregulated or downregulated) (Fig. 1C). Tumors with upregulated UFSP2 showed concomitant UFM1 overexpression, as well as increased UFMylation of target proteins compared with matched normal tissue. In contrast, tumors with downregulated UFSP2 demonstrated decreased UFMylation of target proteins despite levels of UFM1, which were either unchanged (patient 3052) or even upregulated (patient 3010).

Evaluation of UFSP2 protein expression in tumor samples according to clinicopathological characteristics of HNSCC patients revealed significantly reduced UFSP2 levels in tumors larger than 4 cm, tumors with positive extranodal extension (ENE), and tumors with depth of invasion greater than 1 cm, suggesting that decreased UFSP2 expression may be associated with a more aggressive tumor phenotype (Fig. 1D).

Furthermore, altered UFSP2 expression (overexpression or downregulation) was significantly associated with tobacco and alcohol exposure status, with a higher proportion of NSND patients (non-smokers/non-drinkers; all female) in the UFSP2-changed group compared with the unchanged group (37.5% vs. 7.9%; p = 0.014; OR = 7.00, 95% CI: 1.63–27.87; Table 2), highlighting a strong association between UFSP2 dysregulation and the absence of established risk factors.

Table 2: Association between UFSP2 expression and tobacco/alcohol exposure status in HNSCC patients.

UFSP2 Expression	NSND, n (%)	SD, n (%)	OR (95% CI)	*p*-Value
Changed	6 (37.5)	10 (62.5)	7.00 (1.63–27.87)	0.014
Unchanged	3 (7.9)	35 (92.1)	1.00 (reference)	

Note: CI, Confidence Interval; UFSP2, UFM1 Specific Peptidase 2; NSND, patients with non-smoking/non-drinking history; SD, patients with smoking and/or drinking history. *p*-values were obtained by Fisher's exact test. Odds ratio (OR) was calculated using the UFSP2-unchanged group as the reference.

Only one patient in the entire cohort exhibited a p16-positive tumor; however, this patient was concurrently a heavy smoker and heavy alcohol consumer, indicating coexistence of classical etiological factors rather than a purely HPV-driven carcinogenic mechanism. The remaining 53 patients were p16-negative. Consequently, HPV status did not act as a meaningful confounder of the reported associations between UFMylation pathway dysregulation and clinicopathological features in this cohort.

On multivariable analysis pre-specified from the associations in Fig. 1D (Firth penalized-likelihood logistic regression), reduced UFSP2 expression showed approximately two-fold higher odds of tumor size > 4 cm, extranodal extension, and depth of invasion > 1 cm (adjusted OR 1.9–2.1); none reached statistical significance, consistent with the limited power of this cohort (Table 3). The cohort is small and predominantly advanced-stage, limiting statistical power; multivariable associations between UFSP2 dysregulation and clinicopathological features were directionally consistent with our other analyses but did not reach significance, and should therefore be regarded as hypothesis-generating and validated in larger, independent cohorts.

Table 3: Multivariable analysis of reduced UFSP2 and aggressive clinicopathological features (n = 54).

Aggressive Feature (Fig. 1D)	Reduced Events/n	Unadjusted OR (95% CI)	*p*-Value	Adjusted OR (95% CI)†	*p*-Value
Tumor size > 4 cm	17/54	1.97 (0.46–8.08)	0.347	1.94 (0.45–8.10)	0.360
Extranodal extension	21/54	2.19 (0.54–9.22)	0.267	2.10 (0.52–8.90)	0.297
Depth of invasion > 1 cm	36/54	1.68 (0.39–9.80)	0.502	1.93 (0.44–11.92)	0.401

Note: First penalized-likelihood logistic regression; odds ratios (OR) with profile-likelihood 95% Confidence Interval (CI). Exposure pre-specified from Fig. 1D: reduced UFSP2 (≤0.5) vs. not reduced. †Adjusted for established risk-factor exposure (smoker and/or drinker vs. non-smoker/non-drinker). CI, Confidence Interval.

3.2 Stemness Markers Are Overexpressed in the Tissue of Patients with Altered Expression of UFSP2

We have explored the expression of stemness markers (CD133, ABCG2, and OCT4) in patients where UFSP2 was either overexpressed or downregulated. In patients with severe clinical presentation of HNSCC, upregulated UFSP2, CD133, and OCT4 were found to be overexpressed in nearly all examined tumor tissue samples (5/6). In the same group, ABCG2 was overexpressed in 2/6 tumor samples. The analysis of the UFC1 and UBA5 genes revealed their overexpression in almost all analyzed tumor tissues from patients with severe clinical HNSCC manifestations (and upregulation of UFSP2) (Fig. 2A).

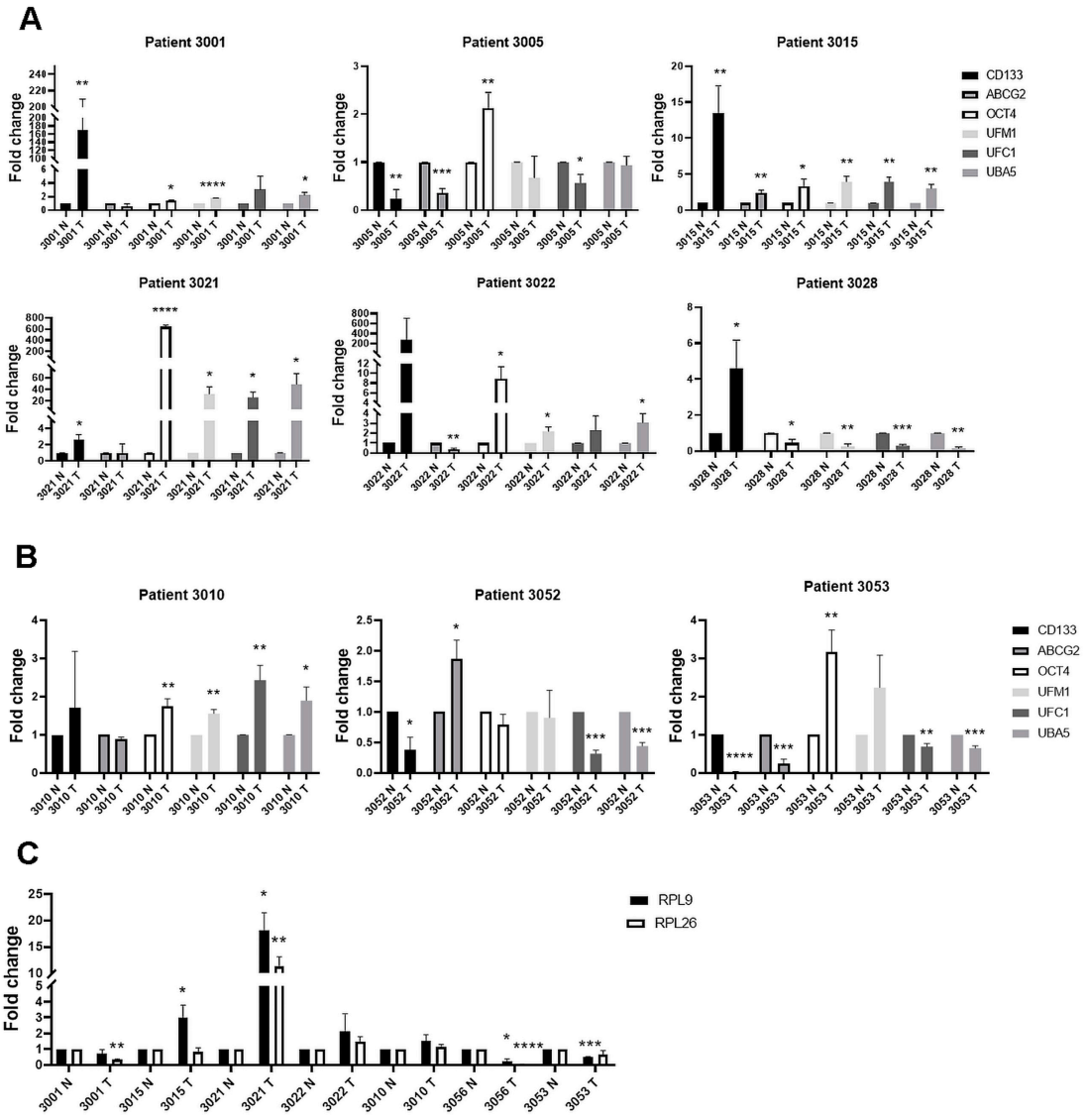

Figure 2: The expression of stemness and UFMylation-related genes in HNSCC tissues of patients with altered UFSP2 expression. (**A**,**B**) Relative mRNA expression levels of stemness markers CD133, ABCG2, OCT4, and UFMylation-related genes UFM1, UFC1, and UBA5 were analysed by qPCR in paired tumor (T) and adjacent normal (N) tissues from HNSCC patients with (**A**) overexpression or (**B**) downregulation of UFSP2 protein. (**C**) Relative mRNA expression levels of UFMylation substrate genes RPL9 and RPL26 measured by qPCR in paired tumor (T) and normal (N) tissues from patients with either overexpressed or downregulated UFSP2 protein. Statistical significance between tumor and normal tissues was evaluated by paired Student's *t*-test (*$p < 0.05$; **$p < 0.01$, ***$p < 0.001$, ****$p < 0.001$; compared to normal tissue). n = 3 independent experiments. CD133, cluster of differentiation 133; ABCG2, ATP-binding cassette subfamily G member 2; OCT4, octamer-binding transcription factor 4; UFM1, ubiquitin-fold modifier 1; UFC1, UFM1-conjugating enzyme 1; UBA5, ubiquitin-like modifier activating enzyme 5; RPL9, ribosomal protein L9; RPL26, ribosomal protein L26.

In the UFSP2-downregulated group, at least one of the examined stemness markers (CD133, ABCG2, and OCT4) was also upregulated in all tested tumor samples. UFMylation genes showed variable expression, distinct from normal tissue, except UFM1 in patient 3052 (Fig. 2B).

RPL9 and RPL26, which are UFMylation target genes (substrates), were also differentially expressed in tumor samples. RPL9 expression was increased in tumor tissue of patients 3015 and 3021 (UFSP2 up-regulated group), but reduced in tumor tissue of patients 3056 and 3053 (UFSP2 down-regulated group). RPL26 expression was reduced in tumor samples of patients 3001 and 3056, but, similar to RPL9, it was strikingly overexpressed in tumor tissue of patient 3021, characterized by high clinical severity (Fig. 2C).

3.3 Lower Concentrations of UBA5 Inhibitor Induce Tumor Sphere Survival While Higher Concentrations Induce Tumor Sphere Cell Death

We have previously shown that UFM1 is overexpressed in CSCs, while its inhibition reduces stemness, epithelial-to-mesenchymal transition (EMT), and CSC survival. Consequently, targeting the UFMylation machinery warrants further investigation into the consequences of its perturbation on CSCs survival and persistence. As UBA5 represents the initiating enzyme essential for the UFMylation pathway activation, we utilized pharmacological inhibition of UBA5 to modulate UFMylation and assess its effects on CSCs. The representative photomicrographs and intracellular ATP levels, as measured by the ViaLight assay, clearly showed that lower concentrations of the UBA5 inhibitor (200–400 μM) promoted tumor sphere survival and proliferation, whereas higher concentrations (800–1600 μM) markedly reduced the formation and survival of tumor spheres (Fig. 3A,B). IC_{50} of UBA5 inhibitor for Detroit 562 tumor spheres was 787 μM. UFMylation status after the treatment of tumor spheres with different concentrations of UBA5 inhibitor showed that UFM1 expression reduces with high concentrations of UBA5 inhibitor, consistent with our qPCR result. However, overall UFMylation of target proteins was increased in spheres after the treatment with the UBA5 inhibitor compared to the untreated control (Fig. 3C).

PARP cleavage was not observed, and levels of other UFMylation proteins remained unchanged after the treatment with 800 μM UBA5 inhibitor (Fig. 3D). Treatment of spheres with 800 μM UBA5 inhibitor reduced the expression of stemness markers and UFMylation genes (Fig. 3E), while the treatment with 400 μM UBA5 inhibitor increased the expression of all these markers, indicating pro-survival signaling (Fig. 3F).

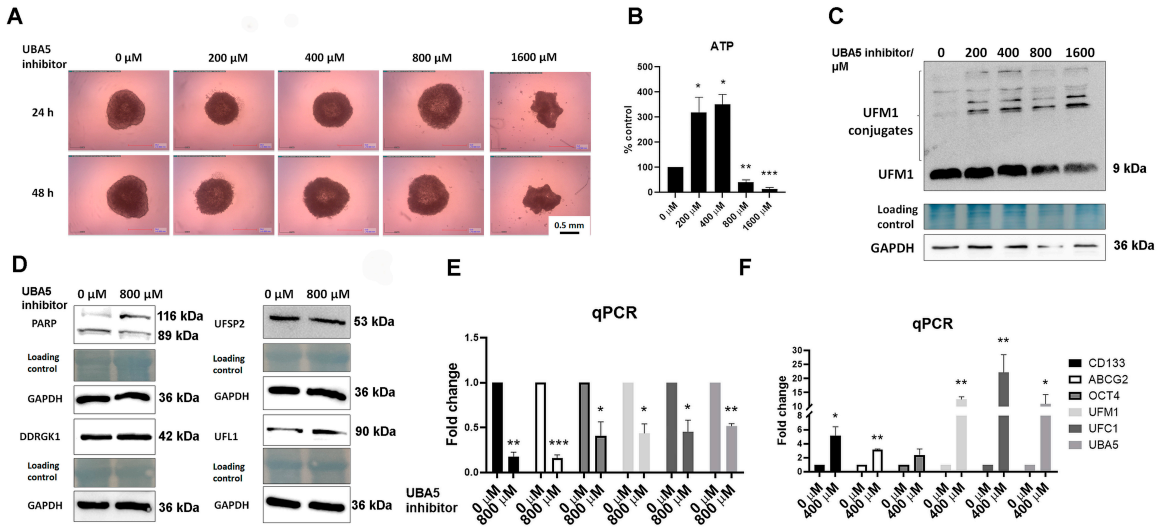

Figure 3: Concentration-dependent effects of UBA5 inhibition on tumor sphere survival and stemness. (**A**) Representative photomicrographs of tumor spheres treated with increasing concentrations of UBA5 inhibitor showing reduced

tumor sphere survival at the highest concentration of UBA5 inhibitor after 24 h and 48 h after treatment. (**B**) Concentration-dependent effect of UBA5 inhibitor on survival of tumor spheres. (**C**) UFMylation status after the treatment of spheres with different concentrations of UBA5 inhibitor. (**D**) The expression of UFMylation pathway proteins DDRGK1, UFSP2, and UFL1 and PARP cleavage in tumor spheres remained mostly unchanged following the treatment with 800 μM UBA5 inhibitor, as shown by Western blot analysis. GAPDH protein expression was used as a loading control. (**E, F**) The expression of stemness markers CD133, ABCG2, OCT4, and UFMylation-related genes UFM1, UFC1, and UBA5 was analysed by qPCR in tumor spheres treated with (**E**) 800 μM and (**F**) 400 μM UBA5 inhibitor. Statistical significance between treatments and untreated control was evaluated by paired Student's *t*-test (*$p < 0.05$; **$p < 0.01$, ***$p < 0.001$; compared to untreated control). n = 3 independent experiments. ATP, adenosine triphosphate; qPCR, quantitative real-time polymerase chain reaction.

3.4 UBA5 Inhibitor Induced Autophagy in Lower Concentrations and Ferroptosis in Higher Concentrations

Given the dose-dependent effects of the UBA5 inhibitor on cell proliferation and survival, we evaluated the autophagy markers in adherent cells and tumor spheres upon treatment with increasing UBA5 inhibitor concentrations to determine whether autophagy mediates cell survival. Adherent cells showed morphological changes even at 200 μM UBA5 inhibitor and complete detachment at 800 μM and 1600 μM UBA5, while tumor spheres were more resistant, with notable dissociation observed only at 1600 μM UBA5 inhibitor (Fig. 4A). The expression of autophagy markers LC3B-I/II was strongest in tumor spheres treated with 400 μM UBA5 inhibitor, and it was higher in untreated tumor spheres than in adherent cells, where no marker expression was detected (Fig. 4B).

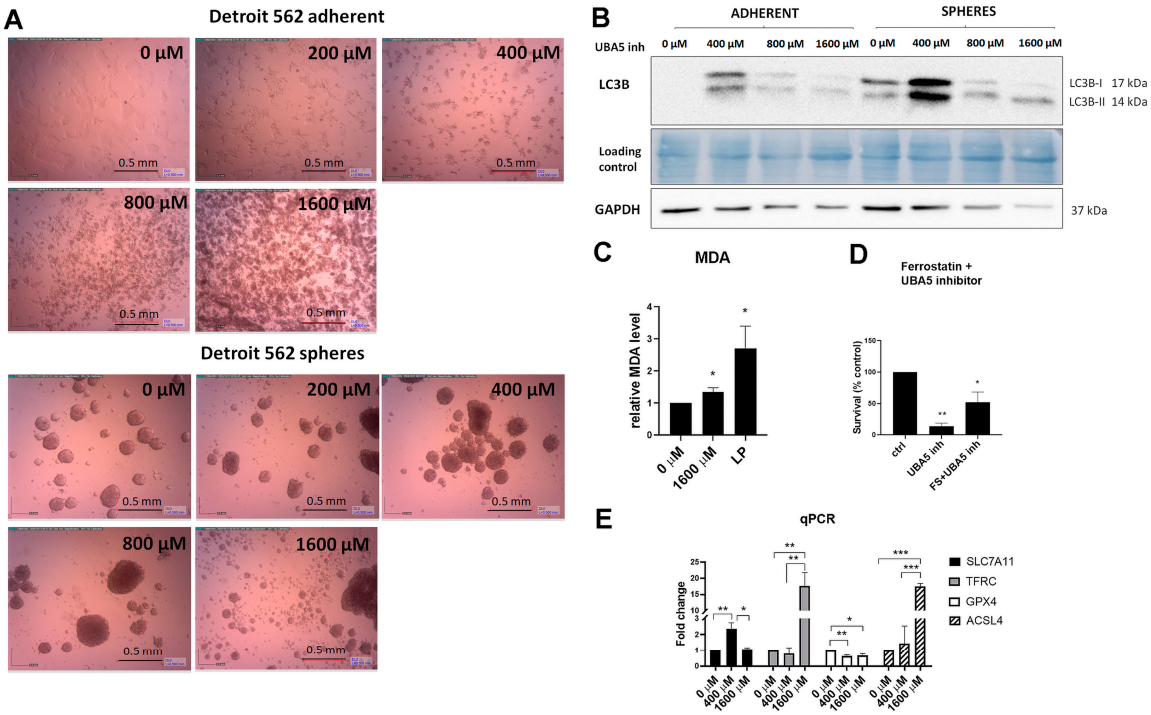

Figure 4: UBA5 inhibitor induces autophagy at lower concentrations and ferroptosis at higher concentrations. (**A**) Representative photomicrographs showing morphological changes in adherent cells and tumor spheres treated

with increasing concentrations of UBA5 inhibitor (200–1600 μM). (**B**) Expression of autophagy markers LC3B-I/II was analysed by Western blot in adherent cells and tumor spheres following treatment with increasing concentrations of UBA5 inhibitor. (**C**) Lipid peroxidation assay showing relative malondialdehyde (MDA) levels in supernatants of tumor spheres treated with 1600 μM UBA5 inhibitor. $CuSO_4$ was used as a positive control to induce lipid peroxidation, and statistical significance between treatment and untreated control was evaluated by paired Student's *t*-test ($^{*}p < 0.05$; compared to untreated control). (**D**) The pre-treatment with 1 μM ferrostatin (FS, ferroptosis inhibitor) followed by a treatment with UBA5 inhibitor for 48 h. Statistical significance between treatments and untreated control was evaluated by paired Student's *t*-test ($^{*}p < 0.05$, $^{**}p < 0.01$). (**E**) The expression of ferroptosis-related genes SLC7A11, TFRC, GPX4, and ACSL4 in tumor spheres treated with 400 μM and 1600 μM UBA5 inhibitor. Statistical significance between treatments and untreated control was evaluated by paired Student's *t*-test ($^{*}p < 0.05$, $^{**}p < 0.01$, $^{***}p < 0.001$; compared to untreated control). n = 3 independent experiments. qPCR, quantitative real-time polymerase chain reaction; MDA: Malondialdehyde.

In light of the evidence linking autophagy and ferroptosis [8,9], we hypothesized that UBA5 inhibition might trigger a similar lethal mechanism in tumor spheres. Treatment of spheres with 1600 μM UBA5 inhibitor increased MDA levels, consistent with elevated lipid peroxidation and ferroptosis. CuSO4 was used as a positive control of lipid peroxidation induction (LP) (Fig. 4C). Pretreatment with ferrostatin-1 (ferroptosis inhibitor) significantly rescued cell survival following UBA5 inhibitor treatment in tumor spheres (Fig. 4D). However, the actual confirmation of ferroptosis came from the qPCR results that showed increased expression of Transferrin receptor protein 1 (TFRC), and Acyl-CoA Synthetase Long Chain Family Member 4 (ACSL4) after the treatment with 1600 μM UBA5 inhibitor. Solute Carrier Family 7 Member 11 (SLC7A11) and Glutathione peroxidase 4 (GPX4) were reduced following the treatment (Fig. 4E). TFRC is involved in iron uptake, which is crucial for ferroptosis, while ACSL4 plays a role in the synthesis of polyunsaturated fatty acids (PUFAs) that are oxidized during ferroptosis. On the other hand, SLC7A11 and GPX4 are key components of the cellular antioxidant defense and are usually reduced during ferroptosis as SLC7A11 is involved in GSH synthesis, and GPX4 prevents lipid peroxidation.

3.5 Bioinformatic Analysis of the Correlation of UBA5 and TfR1/TfR2 with Stemness and EMT Genes

We have previously published that UFM1, unlike other UFMylation proteins, correlates with ZEB, TWIST, and FN1 in HNSCC tumors, but not in control samples [6]. By using GEPIA to analyze correlations between UBA5 and stemness/EMT markers, we have determined that UBA5 expression moderately correlates with stemness markers ALDH1A1 (R = 0.24), KLF4 (R = 0.28), and SOX2 (R = 0.34) in HNSCC tumors, but not in normal tissue. Weaker correlations were observed with stemness markers Nanog (R = 0.11), OCT4 (R = 0.13), and EMT marker ZEB1 (R = 0.12) in tumors, with no significant correlations in normal tissue (Fig. 5).

Bioinformatic analysis further demonstrated that TfR1 and TfR2 expression correlate with important stemness markers (ALDH1A1, SOX2, Bmi-1, MSI2, ABCG2, and ALCAM), additionally supporting the importance of iron uptake in CSCs (Supplementary Fig. S5).

We have also analyzed the correlation between TfR1 and TfR2 and UFMylation genes/proteins and showed that UBA5 moderately correlated with TfR1 (R = 0.38), and TfR2 (R = 0.21) only in HNSCC tumors, whereas DDRGK1 (R = 0.1), UFC1 (R = 0.12), and UFL1 (R = 0.25) showed weaker correlations with TfR1 in HNSCC tumor tissue but not in normal tissue (Supplementary Fig. S6). Further analysis of the TCGA data in GEPIA2 showed that the TfR1 significantly correlates with the pathological disease stages, indicating its prognostic value for HNSCC ($F(3, 515) = 4.34$, $p = 0.0049$) (Supplementary Fig. S7).

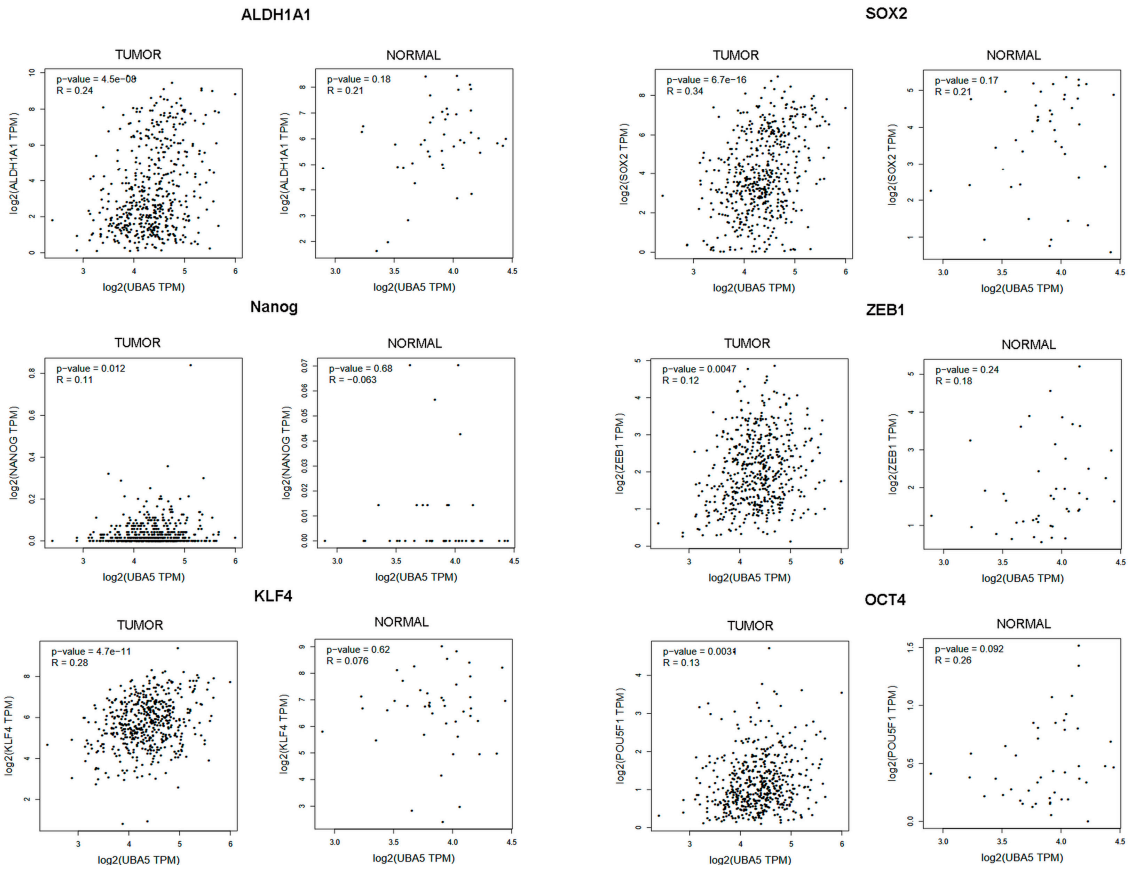

Figure 5: Correlation between UBA5 expression and stemness/EMT markers in HNSCC. Correlation analysis of UBA5 expression with stemness (ALDH1A1, SOX2, and OCT4) and EMT markers (Nanog, ZEB1, and KLF4) in HNSCC using the TCGA data portal and GTEx database through GEPIA. UBA5 expression moderately correlated with stemness markers ALDH1A1 (R = 0.24), KLF4 (R = 0.28), and SOX2 (R = 0.34), and weakly with NANOG (R = 0.11), OCT4 (R = 0.13), and the EMT marker ZEB1 (R = 0.12) in tumor tissues, while no significant correlations were observed in normal tissues. ALDH1A1, aldehyde dehydrogenase 1 family member A1; SOX2, SRY-box transcription factor 2; NANOG, Nanog homeobox; ZEB1, zinc finger E-box binding homeobox 1; KLF4, Kruppel-like factor 4; OCT4, octamer-binding transcription factor 4; UBA5, ubiquitin-like modifier activating enzyme 5; TPM, transcripts per million.

4 Discussion

In the present study, we suggest that dysregulation of the UFMylation pathway is associated with more advanced clinical features of HNSCC. In our cohort of 54 HNSCC patients, UFSP2 expression was highly heterogeneous among examined tumors, with a subset of patients exhibiting either significant overexpression or marked reduction. Interestingly, both overexpression and downregulation were more frequently observed in tumors with severe clinical features, including advanced disease stage (T3 or T4), large tumor size, perineural invasion, bone infiltration, and metastasis. In most cases (75%), UFSP2 overexpression was accompanied by altered DDRGK1 expression. Moreover, reduced UFSP2 expression was significantly associated with larger tumor size, positive extranodal extension, and greater depth of invasion, supporting a link between UFSP2 dysregulation and aggressive HNSCC features. An intriguing observation of our study is the association between altered UFSP2 expression and patient tobacco/alcohol exposure status, with a significantly higher proportion of NSND patients in the group with either overexpressed or downregulated UFSP2 compared to the UFSP2-unchanged group. HNSCC in NSND patients is increasingly

recognized as a biologically and clinically heterogeneous entity, often driven by molecular mechanisms distinct from those underlying tobacco- and alcohol-associated tumors. In this context, our findings suggest that dysregulation of UFMylation may represent one such mechanism contributing to tumor development or progression in this subgroup.

Previous studies have demonstrated that loss of UFSP2 can enhance tumor growth and progression by sustaining UFMylation of oncogenic targets such as ASC1 [10,11], suggesting a tumor suppressor role. However, our findings show that both overexpression and downregulation of UFSP2 may contribute to the aggressiveness of HNSCC, even in patients without established risk factors such as tobacco or alcohol exposure, indicating a complex role of UFSP2 in tumor biology. However, given the relatively small cohort size in each subgroup, these findings should be interpreted cautiously. Future studies in larger, independent cohorts are needed to validate the association between UFSP2 expression and NSND status to assess the potential of UFMylation-related alterations as biomarkers or therapeutic targets.

Our previous work demonstrated that using UFM1 siRNA to target UFMylation decreases EMT and stemness markers (ALDH1A1, CD133, OCT4, ABCG2, FN1, and VIM), while also reducing tumor sphere survival (6). Markers such as CD133, ABCG2, and Oct4 are frequently used to define subpopulations of HNSCC cells with CSC-like properties, including enhanced self-renewal, chemoresistance, and potential for relapse. In OSCC tumors, high CD133 and Oct4 expression correlates with advanced tumor stage and worse prognosis [12,13]. Moreover, Oct4 has also been identified as a reliable marker for detecting radioresistant and cisplatin-sensitive tumors, potentially enabling patient stratification [14]. In addition, ABCG2, often showing co-expression with CD133 in CSC-enriched subpopulations derived from HNSCC patient samples, has been linked to multidrug resistance [15]. A key finding of our study is a correlation between altered UFSP2 levels and the expression of stemness markers. UFSP2 serves as a master regulator of the UFMylation cycle, driving both the maturation of UFM1 and the deUFMylation of target proteins. In the UFSP2-upregulated group, CD133 and Oct4 were upregulated across all examined tumors, while elevated ABCG2 was observed in a subset of patients. Likewise, in the UFSP2-downregulated group, all analyzed tumors showed upregulation of at least one stemness marker, suggesting that dysregulation of UFSP2 may impact the stemness signature of HNSCC cells. One patient (3021) even showed an extreme upregulation of the UFMylation pathway genes (UBA5 112x, UFC1 33x, UFM1 29x, RPL9 18x, and RPL26 11X) paired with high CD133 and OCT4 expression, and an aggressive clinical profile, suggesting possible enrichment of CSCs in this patient. This reinforces the hypothesis that hyper-activation of the UFMylation system is a hallmark of advanced oral cavity tumors. Furthermore, our results demonstrate altered expression of DDRGK1 protein and significantly upregulated expression of other critical UFMylation pathway components, such as UBA5 and UFC1, in tumor tissues of most severe cases, along with heterogeneous expression of target proteins RPL9 and RPL26 among patients. These observations are consistent with earlier studies showing frequent genomic and transcriptional alterations of UFMylation components (UBA5, UFM1, UFL1, and UFC1) in various tumor types [16–18], which, together with our findings, further support the link between dysregulated UFMylation and aggressive tumor phenotypes. To our knowledge, this is one of the first studies demonstrating the expression of UFMylation genes and proteins in HNSCC tissue [19], expanding the evidence that alterations in the UFMylation pathway may play a role in tumor biology across different cancer types.

In our previous study, we demonstrated that UFM1 correlates with EMT markers ZEB, TWIST, and FN1 in tumor tissues compared with normal tissues [6]. The present study extends these observations by showing that UBA5 expression correlates with stemness markers ALDH1A1, KLF4, and SOX2, and to a lesser extent with NANOG, OCT4, and ZEB1, suggesting that UBA5 potentially contributes to the

maintenance of stemness in HNSCC. The fact that these associations were specifically found in tumor tissue but absent in normal tissue indicates tumor-specific function of UBA5. Kumari et al. showed recently that UBA5 levels must be strictly regulated because its overexpression mirrors the phenotype of cells lacking UBA5, suggesting that tight regulation of the UFM1 conjugation enzymes is necessary to ensure the proper directionality of UFM1 transfer [20]. Furthermore, UBA5 can influence the tumor microenvironment as well. It was shown that UBA5 positively correlates with macrophage M2 polarization in lung adenocarcinoma (LUAD) [21]. The knockdown of UBA5 directly suppressed the *in vitro* polarization of macrophages to M2, reduced the *in vivo* infiltration of macrophage M2, and decreased lactate production in LUAD. These results suggest that targeting UBA5 may be a promising therapeutic strategy to reverse the immunosuppressive TME and increase sensitivity to therapy.

Targeting UFMylation via inhibition of UBA5 revealed an unexpected dose-dependent effect. Low concentrations of UBA5 promoted tumor sphere survival, proliferation, and expression of stemness markers, whereas high concentrations significantly reduced sphere viability and led to sphere eradication. Mechanistically, partial UBA5 inhibition induced autophagy in tumor spheres, as evidenced by increased expression of LC3B-I and II, suggesting that suboptimal inhibition of the UFMylation pathway potentially induces mild cellular stress, which may activate pro-survival mechanisms. Basal autophagy promotes renewal and proliferation of CSCs by maintaining their pluripotency [22]. While it can act as a tumor suppressor in early cancer development, in advanced cancers, particularly within the CSC population, autophagy can promote survival, drug resistance, and metastasis. It has already been published that UBA5 inhibitor induces autophagy in breast cancer [23]. In contrast, complete UBA5 inhibition with a high-dose UBA5 inhibitor was accompanied by increased extracellular release of MDA into the culture supernatant, indicating lipid peroxidation and redox stress, processes closely linked to the induction of ferroptosis in cancers. Ferroptosis is an iron-dependent form of regulated cell death and has emerged as a potential targetable weakness in cancer. Cancer cells often upregulate transferrin receptor (TFRC) in order to meet elevated iron demand necessary for increased metabolic activity and proliferation, making ferroptosis a potentially targetable weakness. Increased TfR expression, and consequently iron uptake, is linked to malignancy and the stemness of CSCs derived from hepatocellular carcinoma and other cancers [24]. In our study, we observed increased TFRC and ACSL4 expression alongside reduced expression of SLC7A11 and GPX4, molecular changes characteristic of ferroptotic cell death. Increased ACSL4 expression promotes incorporation of polyunsaturated fatty acids into membrane phospholipids, increasing substrates available for peroxidation and further sensitizing tumor cells to ferroptosis. Simultaneously, downregulation of GPX4 diminishes the cellular capacity to detoxify lipid peroxides, while lower expression of SLC7A11 limits cystine uptake and glutathione synthesis, collectively impairing antioxidant defense and facilitating lipid peroxidation [25]. The survival of CSCs strongly relies on robust anti-ferroptotic defenses, often mediated by upregulation of SLC7A11 and GPX4, and emerging evidence suggests that targeting ferroptosis activation may overcome therapy resistance in HNSCC [24,26].

Beyond mediating iron uptake, TfRs play important roles in maintaining CSC identity, promoting aggressive phenotypes, and contributing to their therapy resistance [27]. Our bioinformatic analyses revealed that TFRC expression significantly correlates with important stemness markers and pathological tumor stage, consistent with previous reports linking TfR1 expression with tumor stage [24], and further supporting the importance of iron uptake in tumor progression and CSC biology, as well as its potential prognostic value.

By optimizing intracellular iron acquisition, TfR1 ensures a sufficient iron pool to support the metabolic demands of CSCs and the enzymatic antioxidant defenses required to mitigate treatment-induced oxidative

stress. While CSCs are generally resistant to apoptosis, emerging research suggests they can be more susceptible to ferroptosis. TfRs are not merely iron transporters in cancer stem cells; they are integral players in maintaining CSC identity, supporting their aggressive behavior, and contributing to their therapy resistance. Given the importance of TfR1 and iron metabolism in CSCs, they may be particularly sensitive to ferroptosis inducers. Ferroptosis activation has been proposed as a strategy to overcome radioresistance in HNSCC by repressing SLC7A11-mediated cystine uptake, depleting GSH, and suppressing GPX4 activity, thereby amplifying tumor cell death when combined with radiotherapy [28]. Furthermore, metformin downregulates SLC7A11 protein stability to induce ferroptosis by inhibiting UFMylation of SLC7A11. Moreover, UFM1 was recently identified as a regulator of ferroptosis in oral squamous cell carcinoma, acting by stabilizing the SLC7A11 protein [19]. Given that SLC7A11 undergoes UFMylation, it is possible that TfR1 is also a substrate, suggesting a broader role for this modification in modulating ferroptosis. However, this should be experimentally verified.

CSCs hoard iron to maintain stemness, creating a highly labile iron pool that also renders them vulnerable to ferroptosis, representing an Achilles' heel that can be therapeutically exploited, for example, with ferroptosis inducers such as a UBA5 inhibitor. Our findings further suggest that UFMylation modulates ferroptosis through regulation of iron homeostasis and redox balance. UFMylation has been reported to stabilize SLC7A11, inhibiting ferroptosis through GSH production and GPX4 activity, but may also promote ferroptosis by facilitating the release of "labile iron" from storage pools [29]. Therefore, therapeutic strategies that exploit iron addiction and ferroptosis sensitivity could represent promising approaches for eliminating CSCs and preventing relapse. However, further mechanistic and *in vivo* studies are required to clarify links with iron metabolism, ribosomal regulation, and the therapeutic potential of UBA5 inhibition.

Several limitations of this study should be acknowledged. First, the patient cohort was relatively small and obtained from a single center, which may limit the broader applicability of the findings. Second, although we identified significant associations between dysregulated UFMylation components, stemness markers, and clinicopathological severity in HNSCCs, the observational nature of the clinical analyses does not establish causality. Third, functional experiments were primarily performed in tumor sphere models, which, although enriched for CSCs, do not fully recapitulate the complexity of the tumor microenvironment *in vivo*. In addition, the molecular mechanisms linking UFMylation to ferroptosis and stemness regulation remain incompletely defined, and the direct UFMylation substrates involved in these processes have not been identified. Finally, larger independent cohorts and *in vivo* studies are needed to further clarify the prognostic and therapeutic relevance of targeting UBA5 and the UFMylation pathway in HNSCC. Our findings provide novel evidence linking UFMylation dysregulation with CSC maintenance and ferroptosis sensitivity in HNSCC.

5 Conclusions

Taken together, our findings provide novel evidence that dysregulation of the UFMylation system contributes to tumor aggressiveness, maintenance of cancer stemness, and modulation of iron metabolism in HNSCC. We hypothesize that UFMylation homeostasis is an important determinant of cellular fate and that dysregulation of this system triggers significant pathological outcomes. From a clinical perspective, dysregulated UFMylation and iron metabolism may represent markers for tumor aggressiveness and therapeutic response. UFSP2 and DDRGK1 expression could support patient stratification and prognosis, while UBA5 may serve as a therapeutic target. The dose-dependent effects of UBA5 inhibition highlight the importance of a delicate balance between survival and death pathways in CSCs when optimizing treatment dose. Considering the established link between autophagy and ferroptosis, further investigation of this axis

may provide additional insights into the mechanisms underlying CSC survival and resistance. In addition, leveraging this axis by carefully optimizing inhibitor concentrations may represent a potential therapeutic strategy to overcome resistance in CSCs.

Acknowledgement: None.

Funding Statement: This work was supported by Croatian Science Foundation (project number: IP-2020-02-4225 Toll-like receptor 3 in the development and treatment of human head and neck cancer: the role of endogenous ligands) and Young Researchers' career development project-training of doctoral students (Croatian Science Foundation).

Author Contributions: Kristina Vukovic Derfi: writing—original draft, review & editing, formal analysis, experimental work; Marko Tarle: writing—original draft, review & editing, formal analysis, sample acquisition; Koraljka Hat: formal analysis, sample acquisition; Tea Vasiljevic: experimental work; Danko Müller: sample acquisition; Ivica Luksic: sample acquisition; Tanja Matijevic Glavan: writing—original draft, review & editing, formal analysis, experimental work, supervision, project administration, funding acquisition. All authors reviewed and approved the final version of the manuscript.

Availability of Data and Materials: The data that support the findings of this study are available from the corresponding author, Tanja Matijevic Glavan, upon reasonable request.

Ethics Approval: The study was conducted in accordance with the Declaration of Helsinki and approved by the Ethics Committee of Clinical Hospital Dubrava, Zagreb, Croatia (No. 2020/2602-02, date: 26.02.2020). Informed patient consent was obtained prior to surgery.

Conflicts of Interest: The authors declare no conflicts of interest.

Supplementary Materials: The supplementary material is available online at https://www.techscience.com/doi/10.32604/or.2026.083630/s1.

Abbreviations

ABCG2	ATP-binding cassette sub-family G member 2
ACSL4	Acyl-CoA Synthetase Long-Chain Family Member 4
ALCAM	Activated Leukocyte Cell Adhesion Molecule
ALDH1A1	Aldehyde Dehydrogenase 1 Family Member A1
ATP	Adenosine triphosphate
Bmi-1	B-lymphoma Mo-MLV insertion region 1 homolog
CSC	Cancer stem cell
DDRGK1	DDRGK domain containing 1
EMT	Epithelial-mesenchymal transition
ENE	Extranodal extension
FS	Ferrostatin
GPX4	Glutathione Peroxidase 4
GSH	Glutathione
HNSCC	Head and Neck Squamous Cell Carcinoma
KLF4	Krüppel-like factor 4
LC3B	Microtubule-associated protein 1 light chain 3 beta
MDA	Malondialdehyde
MSI2	Musashi RNA-binding protein 2
M stage	Metastasis stage
N	Normal tissue
N stage	Node stage
NSND	Non-Smoker, Non-Drinker

OCT4	Octamer-binding transcription factor 4
OSCC	Oral squamous cell carcinoma
PNI	Perineural invasion
PUFAs	Polyunsaturated fatty acids
qPCR	Quantitative real-time polymerase chain reaction
RPL26	Ribosomal Protein L26
RPL9	Ribosomal Protein L9
SLC7A11	Solute carrier family 7 member 11
SOX2	SRY-Box Transcription Factor 2
T	Tumor tissue
TfR1	Transferrin receptor protein 1
TfR2	Transferrin receptor protein 2
TFRC	Transferrin Receptor gene
T stage	Tumor stage
UBA5	Ubiquitin-like modifier-activating enzyme 5
UFC1	Ubiquitin-Fold Modifier Conjugating Enzyme 1
UFL1	UFM1 Specific Ligase 1
UFM1	Ubiquitin-Fold Modifier 1
UFSP1	UFM1 specific peptidase 1
UFSP2	UFM1-Specific Peptidase 2
ZEB1	Zinc finger E-box-binding homeobox 1

References

1. Liu Q, Guo Z, Li G, Zhang Y, Liu X, Li B, et al. Cancer stem cells and their niche in cancer progression and therapy. Cancer Cell Int. 2023;23(1):305. [CrossRef].
2. Millrine D, Peter JJ, Kulathu Y. A guide to UFMylation, an emerging posttranslational modification. FEBS J. 2023;290(21):5040–56. [CrossRef].
3. Hu Z, Wang X, Li D, Cao L, Cui H, Xu G. UFBP1, a key component in ufmylation, enhances drug sensitivity by promoting proteasomal degradation of oxidative stress-response transcription factor Nrf2. Oncogene. 2021;40(3):647–62. [CrossRef].
4. Li Q, Tie Y, Alu A, Ma X, Shi H. Targeted therapy for head and neck cancer: Signaling pathways and clinical studies. Sig Transduct Target Ther. 2023;8(1):31. [CrossRef].
5. Vukovic Đerfi K, Vasiljevic T, Matijevic Glavan T. Recent advances in the targeting of head and neck cancer stem cells. Appl Sci. 2023;13(24):13293. [CrossRef].
6. Derfi KV, Vasiljevic T, Dragicevic T, Glavan TM. Mithramycin targets head and neck cancer stem cells by inhibiting Sp1 and UFMylation. Cancer Cell Int. 2024;24(1):412. [CrossRef].
7. Mikulandra M, Kobescak A, Verillaud B, Busson P, Matijevic Glavan T. Radio-sensitization of head and neck cancer cells by a combination of poly(I:C) and cisplatin through downregulation of survivin and c-IAP2. Cell Oncol. 2019;42(1):29–40. [CrossRef].
8. Gao M, Monian P, Pan Q, Zhang W, Xiang J, Jiang X. Ferroptosis is an autophagic cell death process. Cell Res. 2016;26(9):1021–32. [CrossRef].
9. Chen F, Cai X, Kang R, Liu J, Tang D. Autophagy-dependent ferroptosis in cancer. Antioxid Redox Signal. 2023;39(1–3):79–101. [CrossRef].
10. Yoo HM, Park JH, Jeon YJ, Chung CH. Ubiquitin-fold modifier 1 acts as a positive regulator of breast cancer. Front Endocrinol. 2015;6:36. [CrossRef].
11. Zhou J, Ma X, Xu L, Liang Q, Mao J, Liu J, et al. Genomic profiling of the UFMylation family genes identifies UFSP2 as a potential tumour suppressor in colon cancer. Clin Transl Med. 2021;11(12):e642. [CrossRef].
12. Singh A, Srivastava AN, Akhtar S, Siddiqui MH, Singh P, Kumar V. Correlation of CD133 and Oct-4 expression with clinicopathological and demographic parameters in oral squamous cell carcinoma patients. Natl J Maxillofac Surg. 2018;9(1):8–13. [CrossRef].
13. Fan ZN, Li MX, Chen XB, Wang J, Liang XY, Wang HF, et al. Prognostic value of cancer stem cell markers in head and neck squamous cell carcinoma: A meta-analysis. Sci Rep. 2017;7:43008. [CrossRef].

14. Routila J, Qiao X, Weltner J, Rantala JK, Carpén T, Hagström J, et al. Cisplatin overcomes radiotherapy resistance in OCT4-expressing head and neck squamous cell carcinoma. Oral Oncol. 2022;127:105772. [CrossRef].
15. Lu BC, Li J, Yu WF, Zhang GZ, Wang HM, Ma HM. Elevated expression of Nrf2 mediates multidrug resistance in $CD133^{+}$ head and neck squamous cell carcinoma stem cells. Oncol Lett. 2016;12(6):4333–8. [CrossRef].
16. Wang X, Xu X, Wang Z. The post-translational role of UFMylation in physiology and disease. Cells. 2023;12(21):2543. [CrossRef].
17. Chung CH, Yoo HM. Emerging role of protein modification by UFM1 in cancer. Biochem Biophys Res Commun. 2022;633:61–3. [CrossRef].
18. Song W, He C, Xing X, Xu G, Yao Y, Li H, et al. Targeting the UFL1-PARP1 axis amplifies anti-tumor immunity. Cell Rep. 2025;44(10):116433. [CrossRef].
19. Li G, Yang H, Guo J. UFM1 regulates ferroptosis in oral squamous cell carcinoma by stabilizing SLC7A11. Am J Cancer Res. 2026;16(3):1102–14. [CrossRef].
20. Kumari S, Banerjee S, Kumar M, Hayashi A, Solaimuthu B, Cohen-Kfir E, et al. Overexpression of UBA5 in cells mimics the phenotype of cells lacking UBA5. Int J Mol Sci. 2022;23(13):7445. [CrossRef].
21. Xu D, Zhang D, Wei W, Zhang C. UBA5 inhibition restricts lung adenocarcinoma via blocking macrophage M2 polarization and cisplatin resistance. Exp Cell Res. 2024;440(2):114148. [CrossRef].
22. Li D, Peng X, He G, Liu J, Li X, Lin W, et al. Crosstalk between autophagy and CSCs: Molecular mechanisms and translational implications. Cell Death Dis. 2023;14(7):409. [CrossRef].
23. Fang B, Li Z, Qiu Y, Cho N, Yoo HM. Inhibition of UBA5 expression and induction of autophagy in breast cancer cells by usenamine A. Biomolecules. 2021;11(9):1348. [CrossRef].
24. Xiao C, Fu X, Wang Y, Liu H, Jiang Y, Zhao Z, et al. Transferrin receptor regulates malignancies and the stemness of hepatocellular carcinoma-derived cancer stem-like cells by affecting iron accumulation. PLoS One. 2020;15(12):e0243812. [CrossRef].
25. Zhou Q, Meng Y, Li D, Yao L, Le J, Liu Y, et al. Ferroptosis in cancer: From molecular mechanisms to therapeutic strategies. Sig Transduct Target Ther. 2024;9(1):55. [CrossRef].
26. You H, Wang L, Meng H, Li J, Fang G. Autophagy: Shedding light on the mechanisms and multifaceted roles in cancers. Biomolecules. 2025;15(7):915. [CrossRef].
27. Wang H, Zhang Z, Ruan S, Yan Q, Chen Y, Cui J, et al. Regulation of iron metabolism and ferroptosis in cancer stem cells. Front Oncol. 2023;13:1251561. [CrossRef].
28. Fan L, Shi L, Wang Z, Wang J, Mu Y. Ferroptosis and radiotherapy-related genes in head and neck squamous cell carcinoma: Diagnostic and prognostic significance. Discov Oncol. 2025;16(1):1895. [CrossRef].
29. Yan YX, Zhou HM, Shang XG, Xu P, Tang XQ, Zheng XY, et al. Dynamic regulators of ferroptosis: Post-translational modifications in ferroptotic cell death. Pharmacol Res. 2025;217:107815. [CrossRef].